

Faceting, Grain Growth, and Crack Healing in Alumina

Pankaj Rajak,^{*,†,‡,§,||} Rajiv K. Kalia,^{*,†,‡,§,||} Aiichiro Nakano,^{†,‡,||,§,||} and Priya Vashishta^{†,‡,§,||,||}

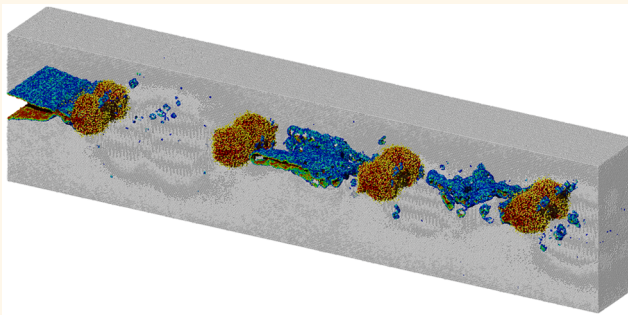
[†]Collaboratory for Advanced Computing and Simulations, [‡]Department of Chemical Engineering & Materials Science, [§]Department of Computer Science, and ^{||}Department of Physics & Astronomy, University of Southern California, Los Angeles, California 90089-0242, United States

Supporting Information

ABSTRACT: Reactive molecular dynamics simulations are performed to study self-healing of cracks in Al_2O_3 containing core/shell SiC/SiO_2 nanoparticles. These simulations are carried out in a precracked Al_2O_3 under mode 1 strain at 1426 °C. The nanoparticles are embedded ahead of the precrack in the Al_2O_3 matrix. When the crack begins to propagate at a strain of 2%, the nanoparticles closest to the advancing crack distort to create nanochannels through which silica flows toward the crack and stops its growth. At this strain, the Al_2O_3 matrix at the interface of SiC/SiO_2 nanoparticles forms facets along the prismatic (A) $\langle\bar{2}110\rangle$ and prismatic (M) $\langle\bar{1}010\rangle$ planes.

These facets act as nucleation sites for the growth of multiple secondary amorphous grains in the Al_2O_3 matrix. These grains grow with an increase in the applied strain. Voids and nanocracks form in the grain boundaries but are again healed by diffusion of silica from the nanoparticles.

KEYWORDS: ceramic nanocomposite, fracture, grain growth, reactive molecular dynamics, self-healing



There is a great deal of interest in designing material systems having the ability to sense and repair damage. Usually damage initiation involves the formation of defects such as dislocations, voids, and microcracks. These defects grow and coalesce to cause material failure. Taking a cue from biology, material scientists are developing novel self-healing systems to enhance reliability and lifetime of materials while reducing the cost of manufacturing, monitoring, and maintenance.^{1–4}

Most of the approaches to designing self-healing material systems involve nanoscale or mesoscale containers filled with a healing material, which is released upon damage initiation either by an external stimulus (heat, light, and electric or magnetic field) or an internal change in the state of the system (pH, stress, or temperature).^{5–8} The healing material is transported to the damage site and immobilized after healing damage. Different materials require different self-healing conditions—ambient conditions for concrete, low temperatures for polymers, relatively high temperatures for metals, and very high temperatures for ceramics.

Here we investigate crack healing in a ceramic nanocomposite operating at high temperatures. Ceramics are lightweight, have high strength and stiffness, and can withstand high temperatures. However, technological applications of ceramics are limited by brittleness and sensitivity to flaws and cracks. Self-healing of defects and cracks can dramatically

increase the reliability and lifetime of ceramics which, in turn, can reduce maintenance costs for a broad range of energy technologies from ceramic turbine blades to solid-oxide fuel cells.^{9,10}

Crack healing has been examined in ceramic nanocomposites consisting of silicon carbide nanoparticles (n-SiC) or SiC whiskers in a silicon nitride (Si_3N_4) matrix^{11,12} and also in an aluminosilicate glass containing vanadium–boride nanoparticles.^{13,14} Experiments have also been carried out to study crack healing in Al_2O_3 by n-SiC.^{15,16} Al_2O_3 has excellent mechanical properties (hardness, wear resistance) and oxidation resistance but low strength ($\sigma_B = 400$ MPa) and low fracture toughness ($K_{IC} = 3$ MPa $\text{m}^{1/2}$). Ando et al. measured the bending strength of sintered $\text{Al}_2\text{O}_3/\text{SiC}$ composites from room temperature to 1300 °C.^{17–20} They introduced indentation cracks on Al_2O_3 surfaces and observed crack healing by n-SiC in the temperature range of 900 °C and 1300 °C. Precracked specimens were found to recover their static and fatigue strengths after crack healing. Three-point bending experiments on crack-healed samples showed the onset of fracture outside the crack-healed zone, whereas samples that had not gone through the crack-healing treatment

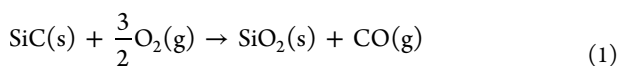
Received: April 3, 2018

Accepted: August 3, 2018

Published: August 3, 2018

fractured just below indentation cracks. Ando et al. have suggested a two-step process of crack healing: First, n-SiC are oxidized by atmospheric oxygen, and a 2–4 nm thick amorphous silica layer is formed around n-SiC; second, heat generated by oxidation and associated volume expansion produce molten silica which diffuses into cracks and heals them. Ando et al. find that the critical concentration of n-SiC for crack healing is between 15 and 20%. Experiments by Niihara et al. indicate that five percent volume fraction of submicrometer size SiC particles can increase the fracture toughness of alumina by 40% and strength by 1 GPa.²¹

In this paper we examine atomistic mechanisms of crack healing in Al_2O_3 by oxidized n-SiC and also grain nucleation and grain growth due to the presence of SiC in Al_2O_3 . Prior to this work, we performed reactive molecular dynamics (RMD) simulation to study oxidation of n-SiC.^{22,23} Nanoparticles were cut out of cubic SiC crystal and placed in an oxygen rich environment. The chemical reaction



led to the formation of silica layers around n-SiC. The first few layers formed rapidly, but the growth slowed down due to limited diffusion of reactants to the n-SiC/SiO₂ interface. The thickness of the silica shell around n-SiC ranged between 2 and 4 nm, depending on the pressure and temperature of the oxygen environment. This is in good agreement with experiments of Ando et al.²⁰

RESULTS

Shapes of cavities in Al_2O_3 change dramatically under strain at 1426 °C. Figure 1a shows a snapshot of an atomic configuration of a cavity containing a n-SiC/SiO₂ nanoparticle (NP). The cavity is no longer spherical. It has facets parallel to prismatic (A) {2̄110} and prismatic (M) {1̄010} planes of crystalline $\alpha\text{-Al}_2\text{O}_3$. These results agree with transmission electron microscopy (TEM) studies of Hockey et al. on faceting of internal cavities in $\alpha\text{-Al}_2\text{O}_3$.²⁴ Analyzing the equilibrium Wulff shapes of cavities annealed at 1600 °C, they found well-developed facets in cavities smaller than 100 nm in diameter. Larger cavities did not exhibit faceting even on experimental time scales. Cavities are an order-of-magnitude smaller in our computer experiments, and therefore nucleation barriers are small enough for faceting transition to manifest on molecular dynamics (MD) time scales. This is consistent with theoretical calculations, which indicate that nucleation barriers for faceting decrease rapidly with a decrease in the cavity size.²⁵

Cavities near the crack facet differently from cavities farther away from the crack. This is due to the stress field of the crack. When the applied strain increases and the crack advances toward nearby cavities, the facets of cavities closest to the crack front first shrink in size and then merge to change the cavity shape from hexagonal to pentagonal; see Figure 1b. These faceting transitions are caused by surface diffusion of Al and O atoms. Our calculations show that surface diffusion coefficients of Al and O are 4×10^{-7} and 2×10^{-7} cm²/s, respectively.

We also observe faceting of n-SiC at 1426 °C, but we do not find any correlation with the facets of alumina cavities in which nanoparticles are embedded. Kaplan et al. have experimentally observed faceting of submicron size SiC particles in internal cavities of $\alpha\text{-Al}_2\text{O}_3$.²⁶ Their high resolution TEM studies reveal that SiC particles develop facets parallel to {1011}, {1014}, and {1012} planes and that these facets have no orientational

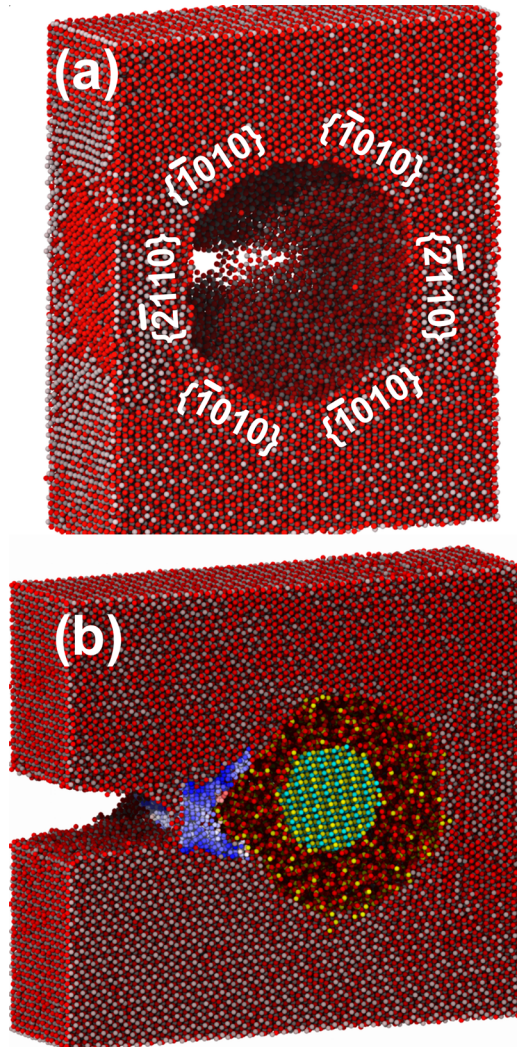


Figure 1. Faceting of an Al_2O_3 cavity around SiC/SiO_2 nanoparticle at 3.4% strain. Here Al_2O_3 contains two rows of SiC/SiO_2 nanoparticles. (a) Al_2O_3 cavity further away from the precrack changes to hexagonal shape while (b) Al_2O_3 cavity near the precrack changes from spherical to pentagonal shape. These facets form along prismatic (A) {2̄110} and prismatic (M) {1̄010} planes.

relationship with facets of alumina cavities which are parallel to {1012}, {1014}, and {0001} planes.

Crack healing begins with the diffusion of molten silica through the pinched-off region of alumina cavities (see Figure 1b). At the onset of crack healing, silica diffuses through nanopores that open up between the crack and the nearest alumina cavities. Unlike bulk, molten silica which consists of SiO₄ tetrahedra, silica in the cavities of alumina at 1426 °C consists of various SiO_x fragments ($x = 0, 1, 2$, and 3). Figure 2a presents an atomic view of crack healing. Here black spheres represent the Al₂O₃ matrix and yellow, red and green spheres are Si, O, and C atoms, respectively. This snapshot, taken at a strain of 4%, shows crack blunting and the presence of SiO_x fragments on crack surfaces. Figure 2b shows the effect of the applied strain on self-diffusion coefficients of SiO_x in the direction of the crack propagation. The diffusion coefficient remains flat and the crack does not propagate for strains less than 2%. Above 2% strain the crack moves toward nanoparticles and self-diffusion coefficients of SiO_x fragments in the

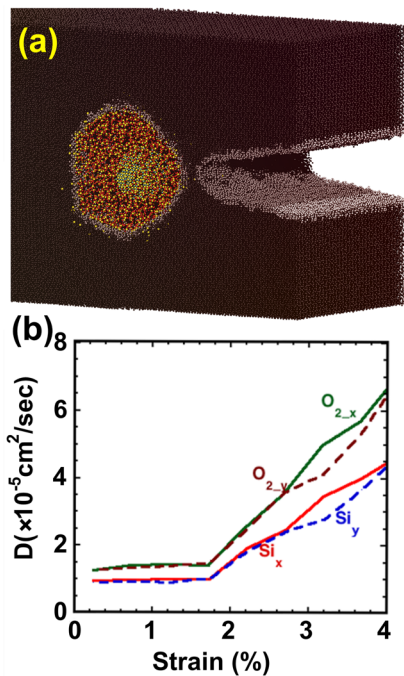


Figure 2. (a) Crack healing in Al_2O_3 by flow of molten silica. Here the alumina matrix is black and yellow, and red and green spheres are Si, O, and C atoms, respectively. The NP diameter is 7 nm and Al_2O_3 contains 1, 2, 3, and 4 rows of NPs. Each row contains 2 NPs of diameter 7 nm separated by 2 nm. (b) Self-diffusion coefficients of Si and O as a function of the applied strain.

direction of approaching crack increase linearly with an increase in the applied strain; see Figure 2b. In addition, n-SiC diffuses into the crack front to stop crack growth. Some of the crack-healing features we observe are similar to those seen in fluorescent imaging of a crack in a silica film evaporated on PMMA containing polymer coated CdSe/ZnS NPs.²⁷ The crack healing mechanism in the experiment involves diffusion of CdSe/ZnS NPs along the interface between silica and PMMA.

We have examined mechanical properties of Al_2O_3 after crack healing. Results for the stress-strain curve and nanoindentation response are presented in Figure S2 in the Supporting Information. The hardness of the crack-healed Al_2O_3 composite is close to the hardness of pure $\alpha\text{-Al}_2\text{O}_3$. This is consistent with the experiment of Ando et al.^{17–20}

We have also examined changes in stress distribution between the crack front and NPs to gain insight into crack arrest and healing by Si and O diffusion. Figure S3b in the Supporting Information displays the stress component σ_{xx} between the crack tip and NPs as a function of the applied strain. The stress increases slightly when the strain is increased to 2%. At higher strains, however, σ_{xx} drops when nanopores nucleate in the alumina matrix between the crack tip and nearby cavities. At a strain of 4%, nanopores coalesce with the precrack and SiO_x fragments diffuse into the crack.

The presence of nanoparticles in faceted cavities gives rise to grain nucleation and grain growth in the strained alumina matrix. Snapshots in Figure 3a–d show nucleation of grains (blue) on facets normal to the direction of crack propagation. These grains are nucleated by the rotation of n-SiC inside the cavities.^{28,29} Inside the grains are under coordinated Al (5-fold) and O (3-fold) atoms due to broken Al–O bonds. Grains

between neighboring n-SiC grow with an increase in the applied strains and coalesce at a strain of 4.4% (see Movie S1). Grain boundaries are amorphous, and they contain nanoscale pores at small strains which grow and coalesce to form secondary cracks at a strain of 4.8%. These cracks are also healed by silica diffusion from cavities.

We have examined stress distribution in the system to gain further insight into grain growth. The top panel in Figure 4a shows the stress component σ_{yy} in the $x-z$ plane of the lower half of the system at an applied strain of 3.4%. (σ_{yy} is time-averaged virial stress in voxels of size 0.5 nm.³⁰) The stress is negligible around n-SiC (see the blue region in the bottom panel) and reaches 15 GPa approximately 10 nm ahead of the first row of n-SiC. The stress decreases away from the first row of nanoparticles and rises again reaching 12 GPa approximately 10 nm ahead of the second row of NPs.

The stress σ_{yy} correlates very well with damage evolution during grain nucleation and grain growth. Local damage³¹ is assessed by calculating the relative displacements of atoms under a uniform strain, ϵ_{ij} :

$$D^2(t, \Delta t) = \sum_{n=1}^N \sum_{i=1}^3 \left\{ r_n^i(t) - r_0^i(t) - \sum_{j=1}^3 [(\delta_{ij} + \epsilon_{ij})(r_n^i(t - \Delta t) - r_0^i(t - \Delta t))] \right\}^2 \quad (2)$$

where

$$\epsilon_{ij} = \sum_k X_{ik} Y_{ik}^{-1} - \delta_{ij} \quad (3)$$

and

$$X_{ij} = \sum_n [r_n^i(t) - r_0^i(t)][r_n^j(t - \Delta t) - r_0^j(t - \Delta t)] \quad (4)$$

$$Y_{ij} = \sum_n [r_n^i(t) - r_0^i(t)][r_n^j(t - \Delta t) - r_0^j(t - \Delta t)] \quad (5)$$

Here r_0 and r_n are atomic coordinates in the unstrained and strained systems, respectively, and the summation over n includes all atoms within the range of interaction. Equation 2 is minimized with respect to ϵ_{ij} to obtain D^2_{min} .

The bottom panel of Figure 4b shows the minimized values of eq 2 along the basal (0001) and prism (2110) planes of a section of Al_2O_3 . Here green and blue regions correspond to $D^2_{min} = 1.5$ and $D^2_{min} = 0.25$, respectively. The maximum deformation occurs along the slip direction [0111] of the prism plane of $\alpha\text{-Al}_2\text{O}_3$ (see Supporting Information Figure S4(a), Movie S2).^{32–34} These deformation values correlate very well with changes in σ_{yy} in the $x-z$ plane.

We have also investigated the effect of three and four rows of NPs on damage mitigation in the alumina matrix. The diameter of each NP (7 nm) and the distance between NPs (2 nm) are kept the same. Recall, with a single row of NPs, silica heals the precrack but damage appears approximately 65 nm ahead of the NPs above a strain of 3.5% and alumina matrix fractures at a strain of 4.5%. A crack develops and propagates on the prism plane along the slip direction [0111] due to the formation and coalescence of nanovoids along the [0111] direction. In the case of two rows of NPs, cracks appear

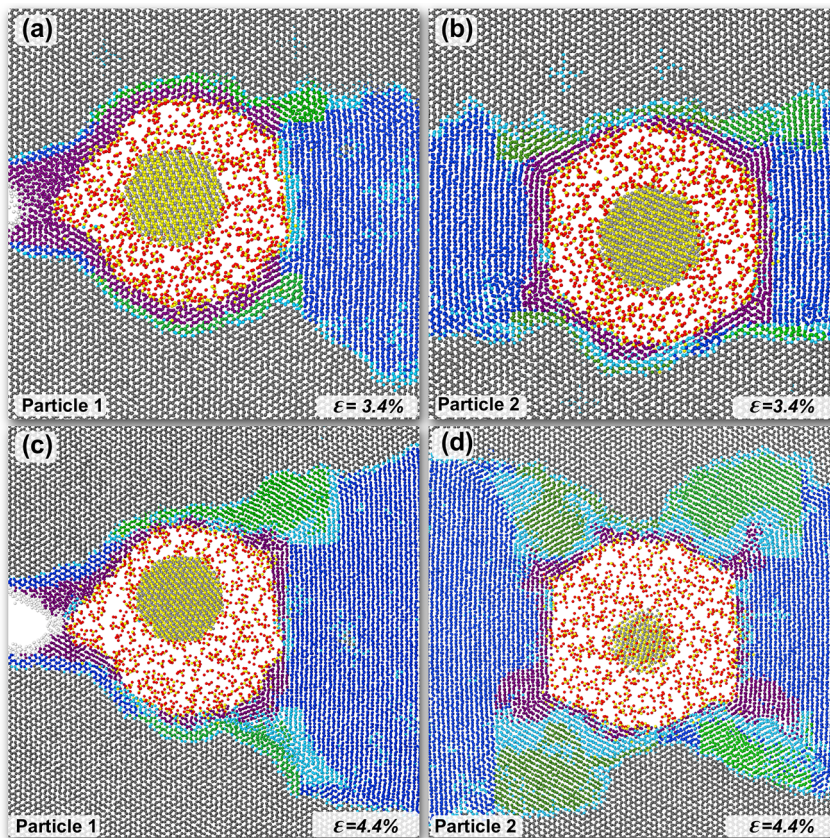


Figure 3. Nucleation and growth of multiple secondary grains at the interface of an Al_2O_3 -n-SiC/SiO₂. Here the Al_2O_3 matrix contains two rows of n-SiC/SiO₂ nanoparticles. Secondary grains form above 3% strain, and facets of the Al_2O_3 cavity act as nucleation sites for these grains. Particle 1 in the figure is in row 1, which is closer to the crack than particle 2 in row 2.

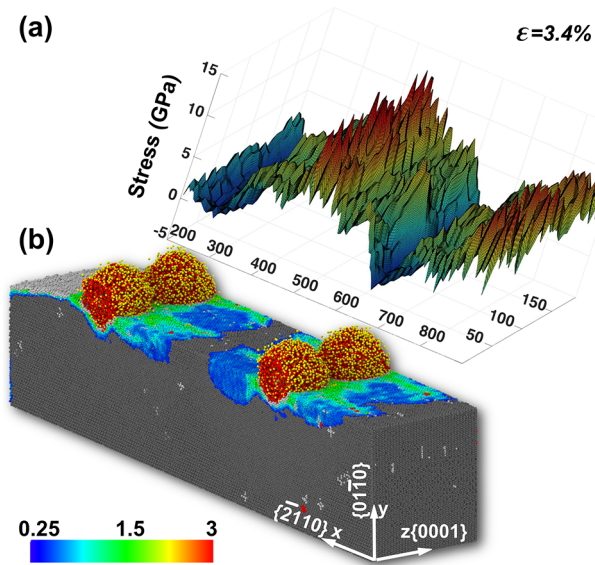


Figure 4. Analysis of stress distribution and local damage inside the Al_2O_3 matrix containing 2 rows of NPs at 3.4% strain. (a) Stress distribution is plotted on a plane at $y = 20$ nm. (b) Local damage on a cross-section of Al_2O_3 at $y = 20$ nm. Here yellow and red are silicon and oxygen atoms, respectively. Al_2O_3 atoms with D^2_{\min} value less than 0.25 are shown in black, and the remaining Al_2O_3 atoms are colored by their D^2_{\min} value.

and propagate directly ahead of the second row of nanoparticles; see Figure 5a and Movie S3. The damage zone starts

around 100 nm ahead of the precrack. Another row of NPs shifts the damage zone further to 130 nm. Finally, with four rows of nanoparticles the system is healed and there are no cracks in the alumina matrix at 5% strain; see Figure 5b and Movie S4. The damage is only in the form of nanovoids in between the rows of n-SiC, but silica diffusion heals them and prevents crack growth. When the strain exceeds 5%, secondary cracks appear in grain boundaries, but they are also healed by silica diffusion from nearby cavities.

CONCLUSION

In summary, RMD simulations of Al_2O_3 containing SiC/SiO₂ nanoparticles show that silica is an excellent healing agent of cracks in alumina at high temperature. When the applied strain is increased, bonds break and nanovoids are formed in the alumina matrix between the crack front and nanoparticles. These nanovoids are the conduits through which silica diffuses into the crack to stop its growth. The self-diffusion coefficient of silica is liquid-like ($>10^{-5} \text{ cm}^2/\text{s}$), and it increases rapidly with an increase in the applied strain. As a result, the higher the applied strain, the more rapid the crack healing. RMD simulations also show that alumina cavities containing SiC/SiO₂ nanoparticle are faceted, and the low energy prismatic (A) {2110} and prismatic (M) {1010} planes are the prominent facets. These results are consistent with TEM studies of nanocavities in α - Al_2O_3 . We observe grain formation on facets and grain growth with an increase in the strain. Damage in the form of nanovoids and nanocracks is observed in grain boundaries, but rapid diffusion of silica from

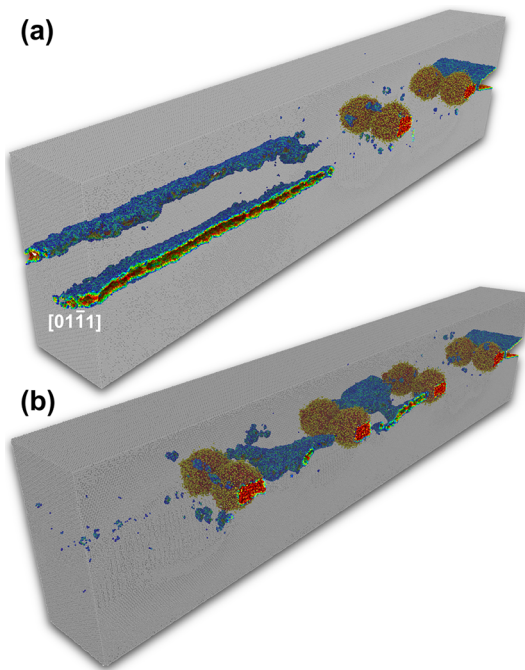


Figure 5. Effect of (a) 2 rows and (b) 4 rows of NPs on crack healing in Al_2O_3 . Here Al_2O_3 atoms are shown in black color and Si and O atoms of NPs are shown in yellow and red, respectively. Atoms near the crack surface or damaged zone are colored by their D_{\min}^2 value. Crack formation happens due to void nucleation and coalescence along the slip direction $[01\bar{1}1]$ of the prism plane of α - Al_2O_3 , as shown in part a.

nanoparticles again heals the damage. The weak link in the strained Al_2O_3 matrix is the $[01\bar{1}1]$ slip direction in the prism plane, along which nanovoids can nucleate and coalesce to form cracks and cause fracture in the $[01\bar{1}1]$ direction. Nanovoid growth can be mitigated by a judicious choice of the size and spatial distribution of SiC/SiO_2 nanoparticles along the slip direction.

METHOD

Figure S1a in Supporting Information shows an initial configuration of an RMD simulation. Initially, the system consists of a precracked α - Al_2O_3 crystal containing oxidized n-SiC inside spherical cavities of radii between 4 and 7 nm. Simulations were performed for one, two, three, and four rows of oxidized n-SiC ($n\text{-SiC}/\text{SiO}_x$). Each row had either two or three nanoparticles along the crack front, i.e., z direction. The center-to-center distances between nearest neighbor n-SiC was between 2 and 4 nm along z and ~ 30 nm along x. The total number of atoms ranged between 6 to 15 million. RMD simulations were performed with force fields that allow bond breaking and bond formation between atoms. The force fields were developed on the basis of density functional theory (DFT) calculations of Al_2O_3 , SiC, and SiO_2 and using experimental data on structural and thermomechanical properties of these systems (see Supporting Information).^{35–37} Equations of motion in RMD simulations were integrated with the velocity Verlet algorithm using a time step of 1 fs. At zero strain, we thermalized the entire system at 1426 °C in the NPT ensemble³⁸ for 20 ps and then further equilibrated the system in the NVE ensemble for 100 ps. Periodic boundary conditions were imposed during equilibration. Subsequently, we turned off the thermostat and applied a uniaxial strain incrementally. The systems were relaxed for 60 ps after each increment of strain (0.25%), which corresponds to an effective strain rate of $3.5 \times 10^7 \text{ s}^{-1}$.

ASSOCIATED CONTENT

Supporting Information

The Supporting Information is available free of charge on the ACS Publications website at DOI: 10.1021/acsnano.8b02484.

Simulation details, description of interaction potential for Al_2O_3 , SiC, and SiO_2 , and structural analysis of alumina inside the amorphous grain (PDF)

Movie showing nucleation and grain grown of amorphous grains (AVI)

Movie showing stress distribution and local damage in Al_2O_3 (AVI)

Movie showing crack propagation in Al_2O_3 containing 2 rows of nanoparticles (AVI)

Movie showing crack propagation in Al_2O_3 containing 4 rows of nanoparticles (AVI)

AUTHOR INFORMATION

Corresponding Authors

*(P.R.) E-mail: rajak@usc.edu.

*(R.K.K.) E-mail: rkalia@usc.edu.

ORCID

Pankaj Rajak: 0000-0002-6344-6056

Aiichiro Nakano: 0000-0003-3228-3896

Priya Vashishta: 0000-0003-4683-429X

Author Contributions

P.R. carried out the MD simulations and analyzed the results. P.R., R.K.K., A.N., and P.V. designed the MD simulation schedule. R.K.K., A.N., and P.V. advised this work. All authors contributed to analyzing the results and writing the manuscript.

Notes

The authors declare no competing financial interest.

ACKNOWLEDGMENTS

The work was supported by the grant DE-SC0018195 funded by the U.S. Department of Energy, Office of Science. Simulations were performed at the Argonne Leadership Computing Facility under the DOE INCITE program and at the Center for High Performance Computing of the University of Southern California.

REFERENCES

- (1) Sottos, N.; White, S.; Bond, I. Introduction: Self-Healing Polymers and Composites. *J. R. Soc., Interface* **2007**, *4*, 347–348.
- (2) Dongare, A. M.; LaMatta, B.; Rajendran, A. M. Strengthening Behavior and Tension–Compression Strength–Asymmetry in Nanocrystalline Metal–Ceramic Composites. *J. Eng. Mater. Technol.* **2012**, *134*, 041003–041003–8.
- (3) Neel, C.; Thadhani, N. Shock and Release Wave Speed of an Alumina Epoxy Composite. *J. Appl. Phys.* **2009**, *106*, 046105.
- (4) Sinnott, S. B.; Dickey, E. C. Ceramic/Metal Interface Structures and Their Relationship to Atomic- and Meso-Scale Properties. *Mater. Sci. Eng., R* **2003**, *43*, 1–59.
- (5) Williams, K. A.; Boydston, A. J.; Bielawski, C. W. Towards Electrically Conductive, Self-Healing Materials. *J. R. Soc., Interface* **2007**, *4*, 359–362.
- (6) Verberg, R.; Dale, A. T.; Kumar, P.; Alexeev, A.; Balazs, A. C. Healing Substrates with Mobile, Particle-Filled Microcapsules: Designing a ‘Repair and Go’ System. *J. R. Soc., Interface* **2007**, *4*, 349–357.
- (7) Hayes, S. A.; Zhang, W.; Branthwaite, M.; Jones, F. R. Self-Healing of Damage in Fibre-Reinforced Polymer-Matrix Composites. *J. R. Soc., Interface* **2007**, *4*, 381–387.

- (8) Kalista, S. J.; Ward, T. C. Thermal Characteristics of the Self-Healing Response in Poly(Ethylene-co-Methacrylic Acid) Copolymers. *J. R. Soc., Interface* **2007**, *4*, 405–411.
- (9) Swallow, J. G.; Woodford, W. H.; Chen, Y.; Lu, Q.; Kim, J. J.; Chen, D.; Chiang, Y. M.; Carter, W. C.; Yildiz, B.; Tuller, H. L.; Van Vliet, K. J. Chemomechanics of Ionically Conductive Ceramics for Electrical Energy Conversion and Storage. *J. Electroceram.* **2014**, *32*, 3–27.
- (10) Chroneos, A.; Yildiz, B.; Tarancón, A.; Parfitt, D.; Kilner, J. A. Oxygen Diffusion in Solid Oxide Fuel Cell Cathode and Electrolyte Materials: Mechanistic Insights from Atomistic Simulations. *Energy Environ. Sci.* **2011**, *4*, 2774–2789.
- (11) Takahashi, K.; Ando, K.; Murase, H.; Nakayama, S.; Saito, S. Threshold Stress for Crack-Healing of $\text{Si}_3\text{N}_4/\text{SiC}$ and Resultant Cyclic Fatigue Strength at the Healing Temperature. *J. Am. Ceram. Soc.* **2005**, *88*, 645–651.
- (12) Ando, K.; Chu, M. C.; Matsushita, S.; Sato, S. Effect of Crack-Healing and Proof-Testing Procedures on Fatigue Strength and Reliability of $\text{Si}_3\text{N}_4/\text{SiC}$ Composites. *J. Eur. Ceram. Soc.* **2003**, *23*, 977–984.
- (13) Coillot, D.; Méar, F. O.; Podor, R.; Montagne, L. Autonomic Self-Repairing Glassy Materials. *Adv. Funct. Mater.* **2010**, *20*, 4371–4374.
- (14) Coillot, D.; Méar, F. O.; Podor, R.; Montagne, L. Influence of the Active Particles on the Self-Healing Efficiency in Glassy Matrix. *Adv. Eng. Mater.* **2011**, *13*, 426–435.
- (15) Thompson, A. M.; Chan, H. M.; Harmer, M. P.; Cook, R. E. Crack Healing and Stress Relaxation in $\text{Al}_2\text{O}_3/\text{SiC}$ “Nanocomposites”. *J. Am. Ceram. Soc.* **1995**, *78*, 567–571.
- (16) Zhao, J.; Stearns, L. C.; Harmer, M. P.; Chan, H. M.; Miller, G. A.; Cook, R. F. Mechanical Behavior of Alumina–Silicon Carbide “Nanocomposites. *J. Am. Ceram. Soc.* **1993**, *76*, 503–510.
- (17) Ando, K.; Kim, B. S.; Chu, M. C.; Saito, S.; Takahashi, K. Crack-Healing and Mechanical Behaviour of $\text{Al}_2\text{O}_3/\text{SiC}$ Composites at Elevated Temperature. *Fatigue Fract. Eng. Mater. Struct.* **2004**, *27*, 533–541.
- (18) Nakao, W.; Ono, M.; Lee, S.-K.; Takahashi, K.; Ando, K. Critical Crack-Healing Condition for SiC Whisker Reinforced Alumina under Stress. *J. Eur. Ceram. Soc.* **2005**, *25*, 3649–3655.
- (19) Osada, T.; Nakao, W.; Takahashi, K.; Ando, K.; Saito, S. Strength Recovery Behavior of Machined $\text{Al}_2\text{O}_3/\text{SiC}$ Nano-composite Ceramics by Crack-Healing. *J. Eur. Ceram. Soc.* **2007**, *27*, 3261–3267.
- (20) Osada, T.; Nakao, W.; Takahashi, K.; Ando, K. Kinetics of Self-Crack-Healing of Alumina/Silicon Carbide Composite Including Oxygen Partial Pressure Effect. *J. Am. Ceram. Soc.* **2009**, *92*, 864–869.
- (21) Niihara, K. New Design Concept of Structural Ceramics - Ceramic Nanocomposites. *J. Ceram. Soc. Jpn.* **1991**, *99*, 974–982.
- (22) Nomura, K.; Kalia, R. K.; Li, Y.; Nakano, A.; Rajak, P.; Sheng, C.; Shimamura, K.; Shimojo, F.; Vashishta, P. Nanocarbon Synthesis by High-Temperature Oxidation of Nanoparticles. *Sci. Rep.* **2016**, *6*, 24109.
- (23) Newsome, D. A.; Sengupta, D.; Foroutan, H.; Russo, M. F.; van Duin, A. C. T. Oxidation of Silicon Carbide by O_2 and H_2O : A ReaxFF Reactive Molecular Dynamics Study, Part I. *J. Phys. Chem. C* **2012**, *116*, 16111–16121.
- (24) Choi, J.-H.; Kim, D.-Y.; Hockey, B. J.; Wiederhorn, S. M.; Handwerker, C. A.; Blendell, J. E.; Carter, W. C.; Roosen, A. R. Equilibrium Shape of Internal Cavities in Sapphire. *J. Am. Ceram. Soc.* **1997**, *80*, 62–68.
- (25) Mullins, W. W.; Rohrer, G. S. Nucleation Barrier for Volume-Conserving Shape Changes of Faceted Crystals. *J. Am. Ceram. Soc.* **2000**, *83*, 214–16.
- (26) Kaplan, W. D.; Levin, I.; Brandon, D. G. Significance of Faceting on SiC Nanoparticles in Alumina. *Mater. Sci. Forum* **1996**, *207–209*, 733–736.
- (27) Gupta, S.; Zhang, Q.; Emrick, T.; Balazs, A. C.; Russell, T. P. Entropy-driven Segregation of Nanoparticles to Cracks in Multi-layered Composite Polymer Structures. *Nat. Mater.* **2006**, *5*, 229.
- (28) Upmanyu, M.; Srolovitz, D. J.; Lobkovsky, A. E.; Warren, J. A.; Carter, W. C. Simultaneous Grain Boundary Migration and Grain Rotation. *Acta Mater.* **2006**, *54*, 1707–1719.
- (29) Wang, Y. B.; Li, B. Q.; Sui, M. L.; Mao, S. X. Deformation-Induced Grain Rotation and Growth in Nanocrystalline Ni. *Appl. Phys. Lett.* **2008**, *92*, 011903.
- (30) Thompson, A. P.; Plimpton, S. J.; Mattson, W. General Formulation of Pressure and Stress Tensor for Arbitrary Many-Body Interaction Potentials under Periodic Boundary Conditions. *J. Chem. Phys.* **2009**, *131*, 154107.
- (31) Falk, M. L. Molecular-Dynamics Study of Ductile and Brittle Fracture in Model Noncrystalline Solids. *Phys. Rev. B: Condens. Matter Mater. Phys.* **1999**, *60*, 7062–7070.
- (32) Zhang, C.; Kalia, R. K.; Nakano, A.; Vashishta, P.; Branicio, P. S. Deformation Mechanisms and Damage in α -Alumina under Hypervelocity Impact Loading. *J. Appl. Phys.* **2008**, *103*, 083508.
- (33) Heuer, A. H.; Lagerlöf, K. P. D.; Castaing, J. Slip and Twinning Dislocations in Sapphire (α - Al_2O_3). *Philos. Mag. A* **1998**, *78*, 747–763.
- (34) Lagerlöf, K. P. D.; Heuer, A. H.; Castaing, J.; Rivière, J. P.; Mitchell, T. E. Slip and Twinning in Sapphire (α - Al_2O_3). *J. Am. Ceram. Soc.* **1994**, *77*, 385–397.
- (35) Vashishta, P.; Kalia, R. K.; Nakano, A.; Rino, J. P. Interaction Potentials for Alumina and Molecular Dynamics Simulations of Amorphous and Liquid Alumina. *J. Appl. Phys.* **2008**, *103*, 083504.
- (36) Vashishta, P.; Kalia, R. K.; Nakano, A.; Rino, J. P. Interaction Potential for Silicon Carbide: A Molecular Dynamics Study of Elastic Constants and Vibrational Density of States for Crystalline and Amorphous Silicon Carbide. *J. Appl. Phys.* **2007**, *101*, 103515.
- (37) Vashishta, P.; Kalia, R. K.; Rino, J. P.; Ebbsjö, I. Interaction Potential for SiO_2 : A Molecular-Dynamics Study of Structural Correlations. *Phys. Rev. B: Condens. Matter Mater. Phys.* **1990**, *41*, 12197–12209.
- (38) Berendsen, H. J. C.; Postma, J. P. M.; van Gunsteren, W. F.; DiNola, A.; Haak, J. R. Molecular Dynamics with Coupling to an External Bath. *J. Chem. Phys.* **1984**, *81*, 3684–3690.